VISIBLE CAMERA BASED DIAGNOSTICS TO STUDY NEGATIVE ION BEAM PROFILES IN ROBIN

Presented by:
Mr Sidharth Kumar Dash

Co-authors:
Dr. Mainak Bandyopadhyay
Mr Kaushal Pandya
Mr Manas Bhuyan
Mr Ratnakar Yadav
Mr Hiren Mistri
Dr. Mahendrajit Singh

Outline of Talk

- Motivation
- Data Extraction and Sorting
- Models for Analysis
- Comparison with established diagnostics
- Perceiving the discontinuity
- Beam Modelling to bridge the results
- Results Comparison
- Summary

Motivation

Negative ion based beam sources are extensively developed and optimized for use in fusion reactors, due to proven neutralization efficiency in high energy regimes.

One of the intrinsic problems in negative ion beam sources is the plasma asymmetry across the plasma-grid introduced due to the magnetic filter field and bias voltage [1] .

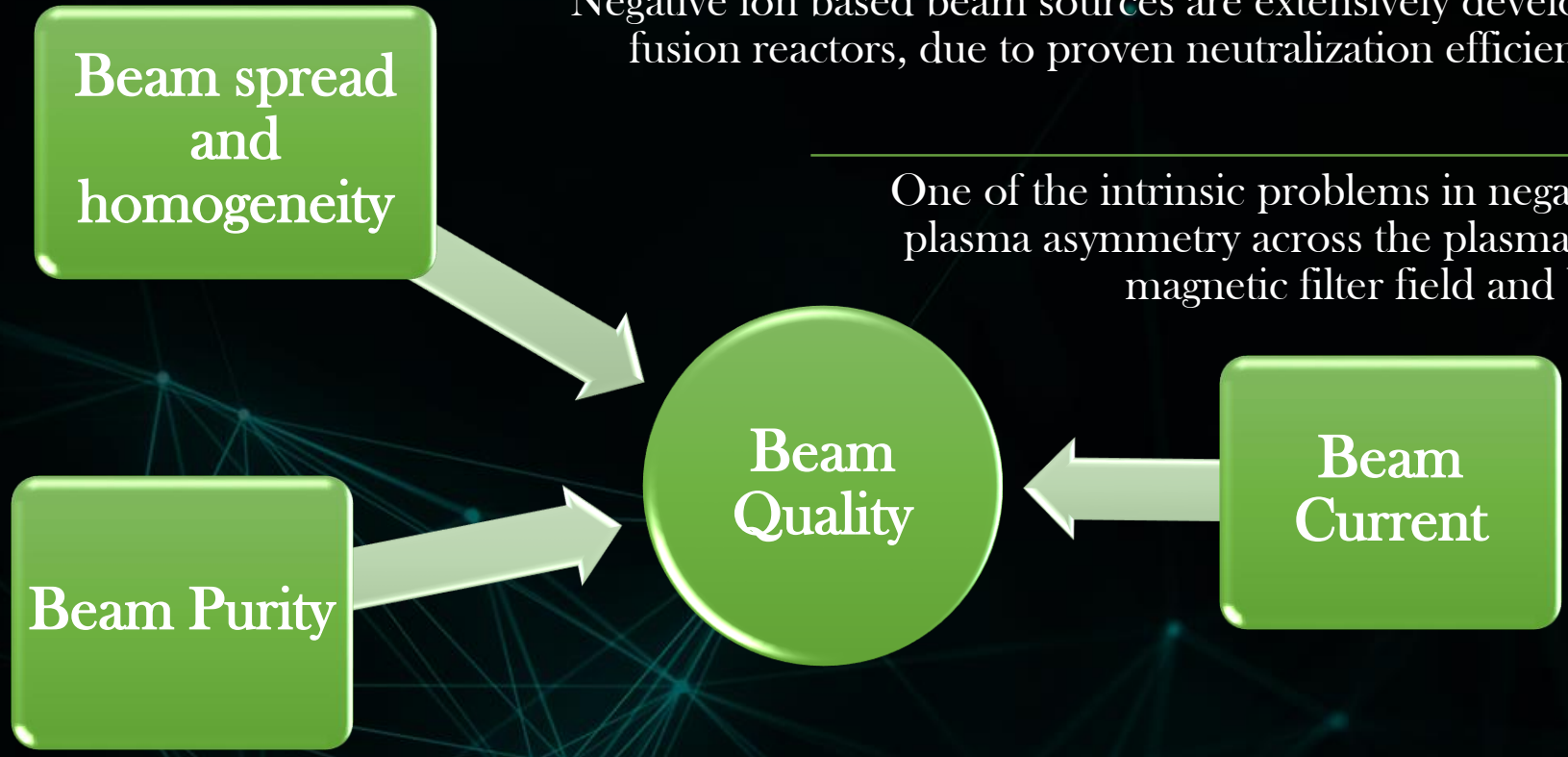

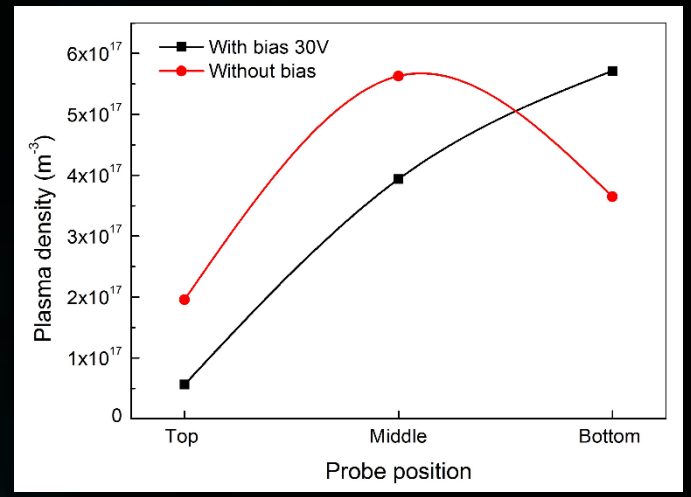

This work deals with diagnosing the beam during transport using a CCD based visible camera and look out for any evidence related to the plasma asymmetry in beam.

1. *M. Bandyopadhyay, et al . "Overview of diagnostics on a small-scale RF source for fusion (ROBIN) and the one planned for the diagnostic beam for ITER." Rev Sci Instrum 1 February 2022; 93 (2): 023504.*

System Description

ROBIN stands for RF-Operated Beam source in India for Negative ions. It uses a 100kW generator with 1MHz frequency to deliver RF power through a single driver and produces maximum current density of 25 mA/cm^2 [1].

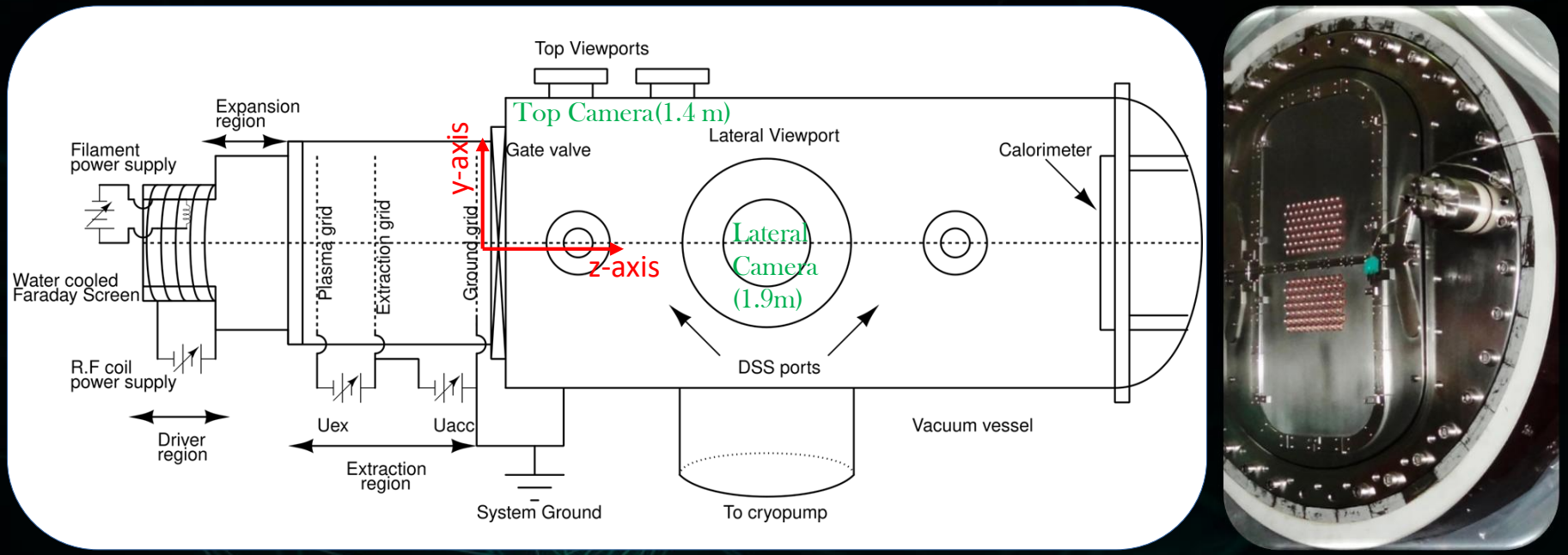

(a)

(b)

Figure 1: a) Schematic diagram representing various components of the ROBIN device b) original picture of the Extraction grid

Langmuir probe and OES are used to probe plasma characteristics while the DSS, thermocouple based calorimeter and two visible range CCD cameras characterize the extracted ion beam.

The device ignites hydrogen plasma and extracts H^- ion beam through a masked Large Area Grid(LAG) system.

1. *M. Bandyopadhyay, et al . "Overview of diagnostics on a small-scale RF source for fusion (ROBIN) and the one planned for the diagnostic beam for ITER." Rev Sci Instrum 1 February 2022; 93 (2): 023504.*

Data Extraction and Sorting

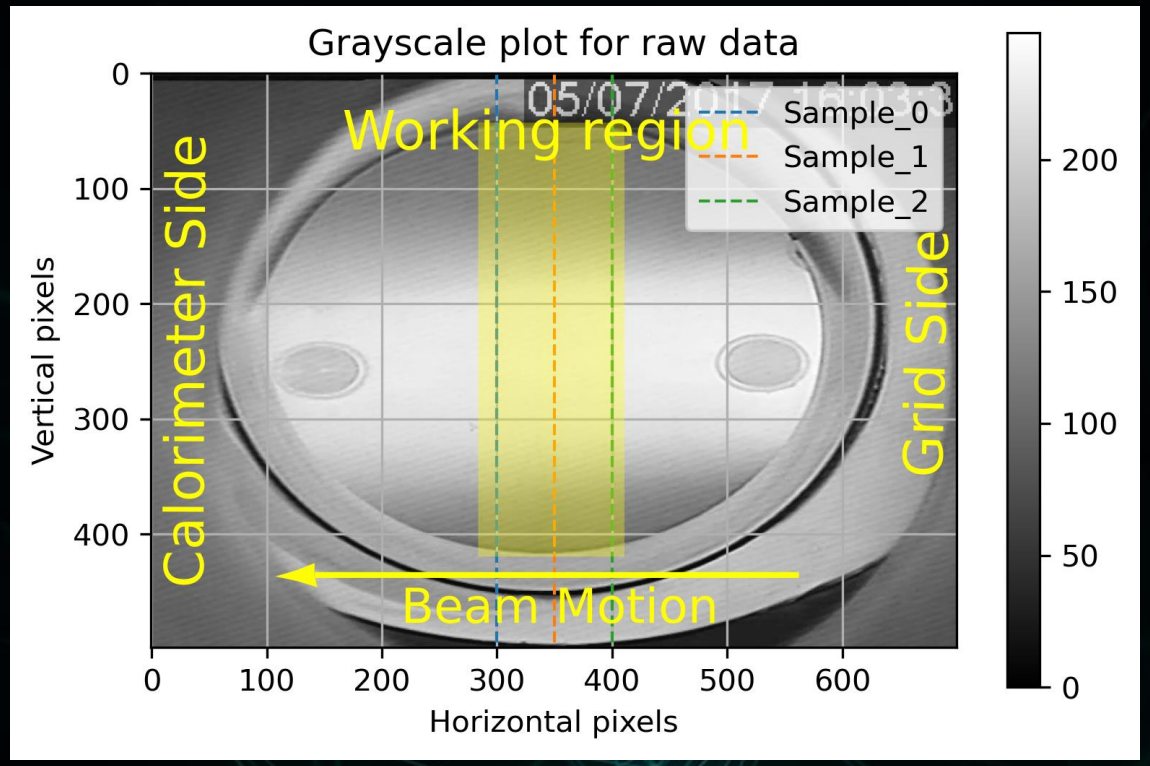

Figure 2: Plot for cropped raw data (*500×700* pixels) in grayscale depicting the orientation and pixel dimensions.

The optical emissions from beam-gas interaction lies within the visible range (400-700 nm), creating the scope for realizing a non-invasive diagnostic[2].

The raw data was recorded using a 20fps CCD based SAMSUNG camera, with 1/3' sensor area and *576×928* pixels.

Theory of perspective projection was used for calibration of camera to from pixel co-ordinates to space co-ordinates.

A region of minimum distortion and maximum usable vertical range (812 mm) was identified as the working region and sampling locations are indicated by dashed lines.

2. M. Ugoletti, et al , "Visible cameras as a non-invasive diagnostic to study negative ion beam properties." Rev Sci Instrum 1 April 2021, 92 (4): 043302.

Scaling Extraction Period

The working region was scanned for whole extraction period and a suitable time range was determined for averaging.

This method helps verify the time synchronization of datasets.

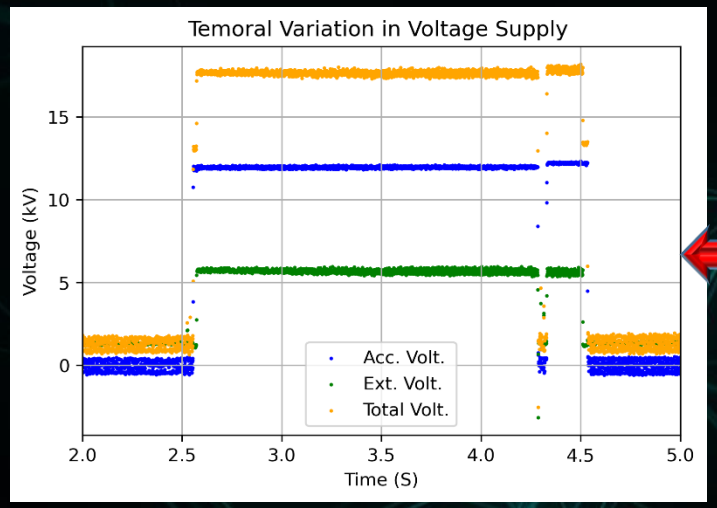

Figure 3: Temporal variation in HV power supply for beam extraction and acceleration.

The total extraction time was ~2s with the rise , fall and fluctuations being significantly visible.

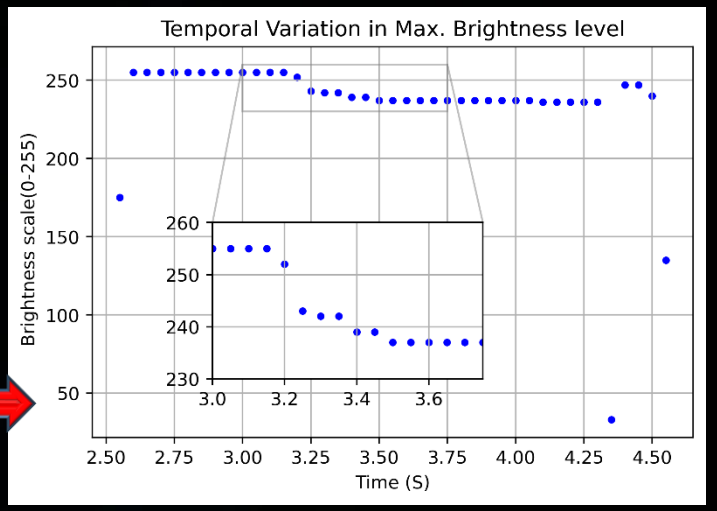

Figure 4: Temporal variation of maximum intensity in working region of lateral camera data.

The dynamic range of camera limits data capture for first few hundred milliseconds, but the emissions fall within range afterwards.

The temporal averaging slot was determined to be 250 ms within the stable regime.

Sample Analysis Models

Model-1(Pure-Gaussian Distribution): The beam from individual grids have merged and formed a perfect Gaussian distribution which may be directly used for estimation of beam parameters[3].

$$f(x) = A * exp(-(x-\mu)^2 / 2\sigma^2) + t \quad ...(1)$$

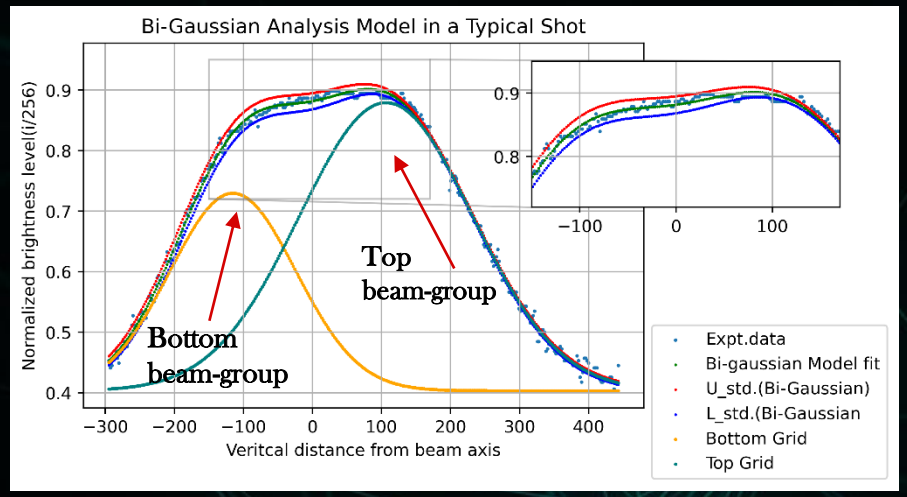

Figure 6: Fitting the spatial emission profile with a bi-Gaussian function, with resolved beam-group Gaussians(χ^2=0.043).

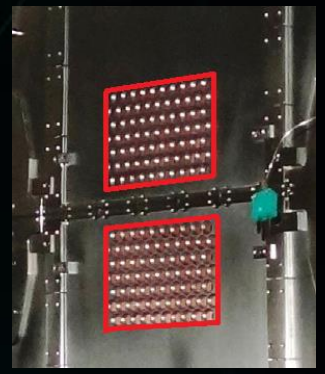

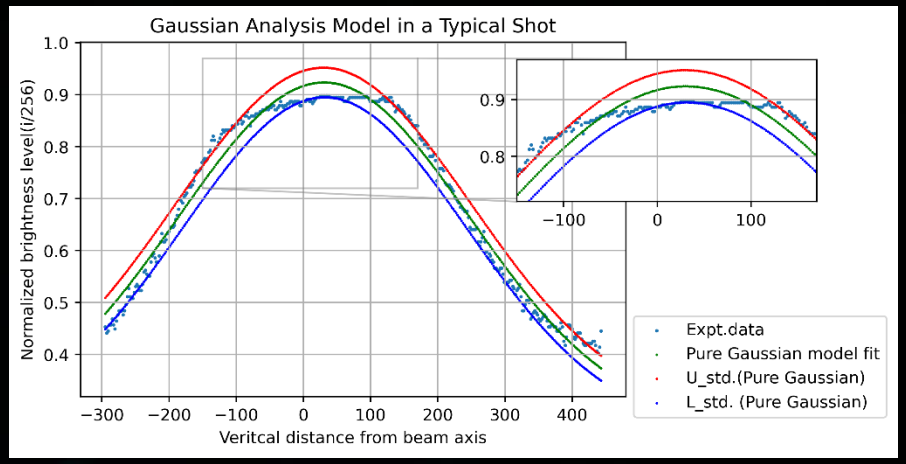

Figure 5: Fitting the spatial emission profile with pure Gaussian function(χ^2=0.346).

Model-2(Bi-Gaussian with close peaks): The emission profile is a linear superposition of two closely spaced Gaussian functions forming a top base with asymmetric Gaussian wings[4].

$$f(x) = A_1 * exp(-(x-\mu_1)^2/2\sigma_1^2) + A_2 * exp(-(x-\mu_2)^2/2\sigma_2^2) + t \quad ...(2)$$

3. Pandya, Kaushal, et al. "First results from negative ion beam extraction in ROBIN in surface mode." In AIP Conference proceedings, vol. 1869, no. 1, AIP Publishing, 2017.

4. D. Borah, et al. "Design of tomographic diagnostic system for Indian Test Facility (INTF) neutral beam injector." Fusion Engineering and Design, Volume 148, 2019, 111255, ISSN 0920-3796.

Validity of Model

The beam intensity ($I(x,y,z)$) for a rectangular ($2W \times 2L$) aperture distribution with a 2-D Gaussian beamlet approximation may be calculated at any point down beamline as[5]:

$$I(x,y,z) = A\{Erf[(W-x)/a_x]+Erf[(W-x)/a_x]\}\{Erf[(L-y)/a_y]+Erf[(L-y)/a_y]\} \quad \ldots(3)$$

Where, $a_x = a_{0x} + z*\tan(\delta_x)$ and $a_y = a_{0y} + z*\tan(\delta_y)$

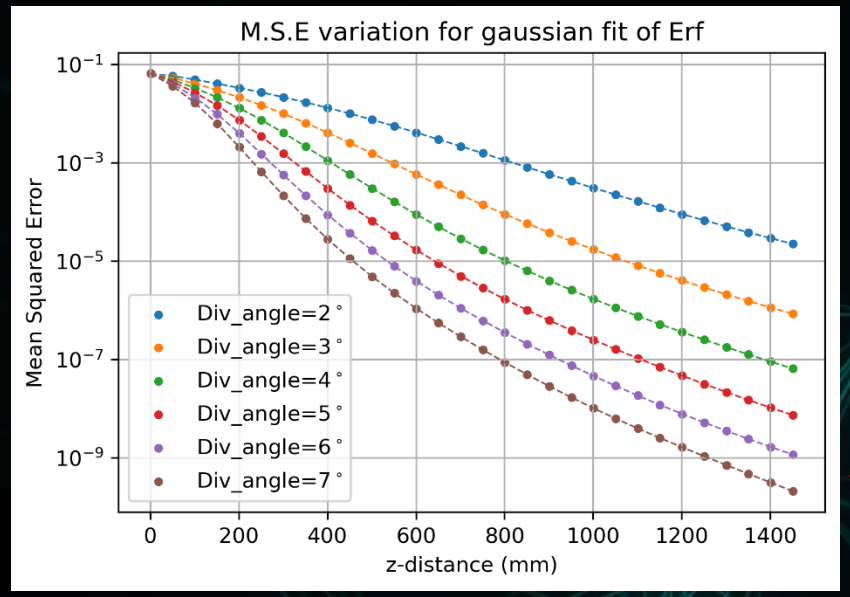

Figure 7: Plot for variation of error in fitting of the Gaussian function and ERF to justify use of bi-Gaussian model.

A plot for *equation(3)* was evolved along z with dimensions of ROBIN and was fitted using a Gaussian function. The Mean Squared Error(MSE) for the fit was plotted for different z-values and for different divergence values.

$$MSE = (1/n)\,\Sigma^{n}_{i=1}\,(y_i - y'_i)^2 \quad \ldots(4)$$

Visual Illustration of evolution

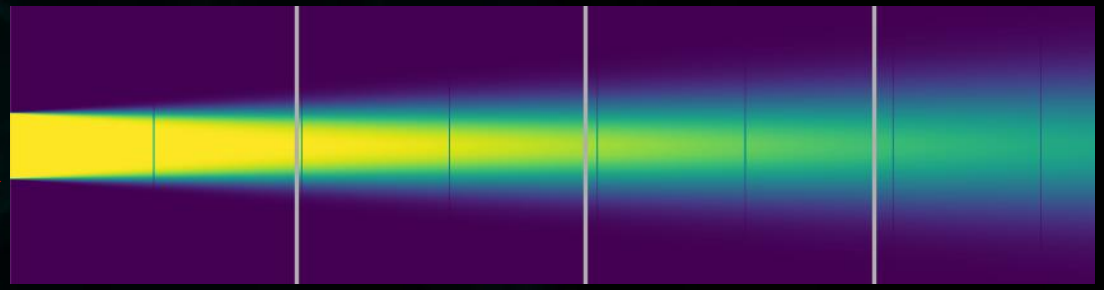

5. Deka, A. J., et al. "Evaluation of beam divergence of a negative hydrogen ion beam using Doppler shift spectroscopy diagnostics." Journal of Applied Physics 123, no. 4 (2018), .

Tracking Divergence Change

The divergence of beam was tracked for a voltage sweep of Extraction voltage (U_{ext}) from 5-17 kV keeping the acceleration voltage (U_{acc}) constant at 5 kV, and the results from lateral camera and calorimeter are compared.

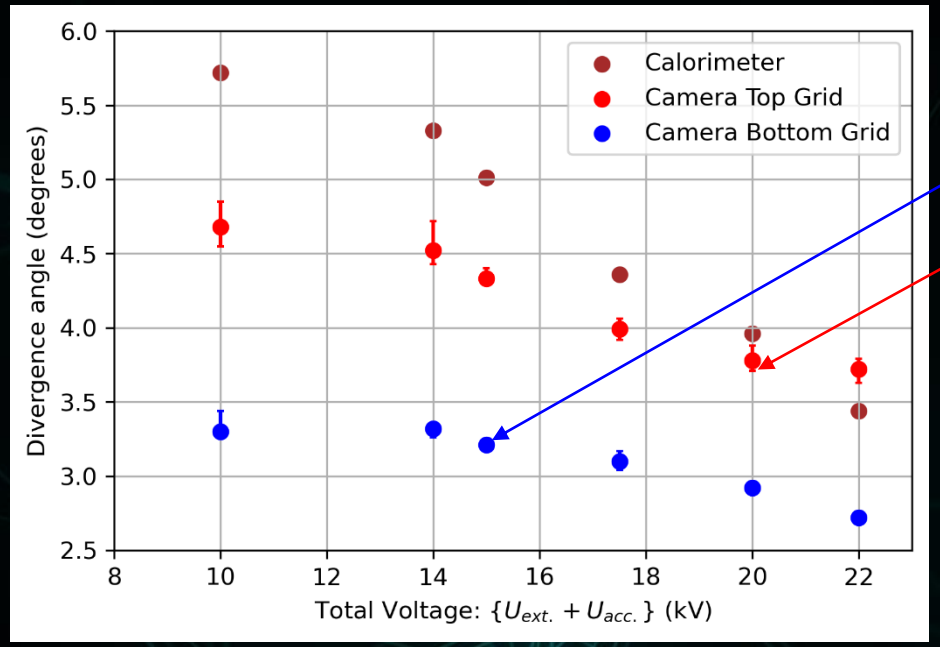

Figure 8: Variation of beam divergence w.r.t extraction voltage(U_{ext}) sweep from 5-15 kV keeping acceleration Voltage (U_{acc}) constant at 5 kV.

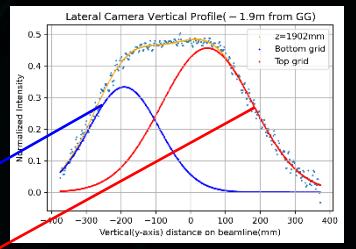

The variation trend is in good agreement for both the top and bottom grid beams resolved data, but the asymmetry is constant for voltage sweep.

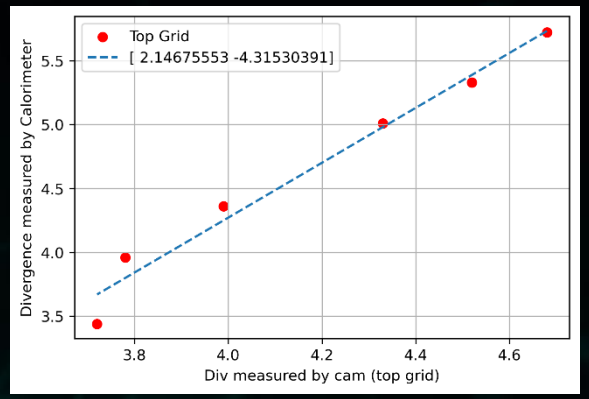

(a)

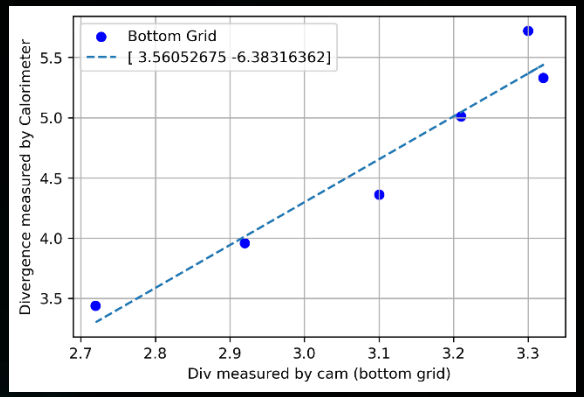

(b)

Figure 9: The variation of divergence measured by calorimeter w.r.t the variation measured by lateral camera a) top grid b)bottom grid.

Beam Modelling

Assuming each extracted beamlet with a Gaussian intensity distribution in the x-y plane and the motion of beam along the z-axis[6].

$$i_{beamlet}(x,y,z) = (i_t/\pi a_x a_y) * exp(-x^2/a_x^2 - y^2/a_y^2) \quad \ldots(5)$$

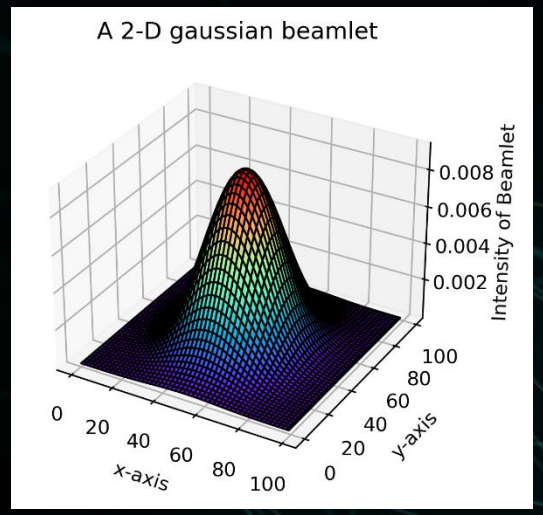

Figure 11: A plot for 2-D Gaussian beamlet

The divergence or 1/e width of maxima is determined by lensing formed by grid apertures and evolves along beamline as:

$$a_x = z \tan(\alpha), \; a_y = z \tan(\beta)$$

The total beam profile obtained by integrating over while emitting area($2W \times 2L$) as:

$$i_{Beam}(x,y,z) = \int_{-w}^{+w} \int_{-l}^{+l} (i_t/\pi a_x a_y) \exp(-(x-x_o)^2/a_x^2 - (y-y_o)^2/a_y^2)\, dx'\, dy' \quad \ldots(6)$$

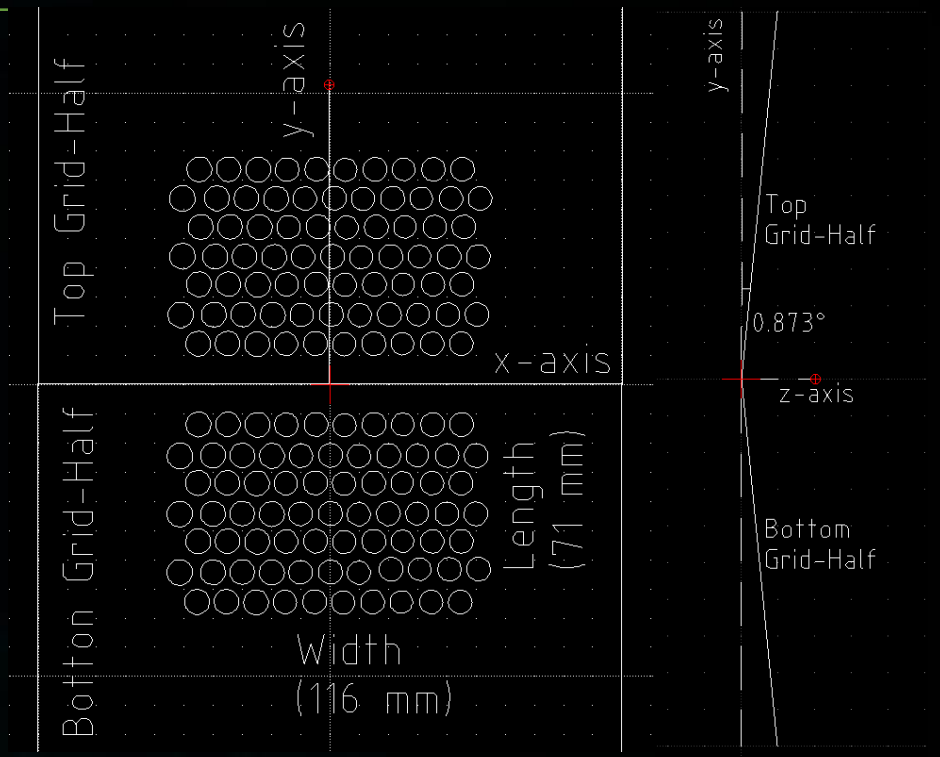

Figure 12: Geometrical description of acceleration grid for simulation

6. Kim, Jinchoon, and J. H. Whealton. "Beam intensity distributions in neutral beam injection systems." Nuclear instruments and methods 141, no. 2 (1977): 187-191.

Geometrical Inputs

As the grid is divided into two halves(top and bottom) and are tilted towards the beam axis with an angle of 0.873^{o}

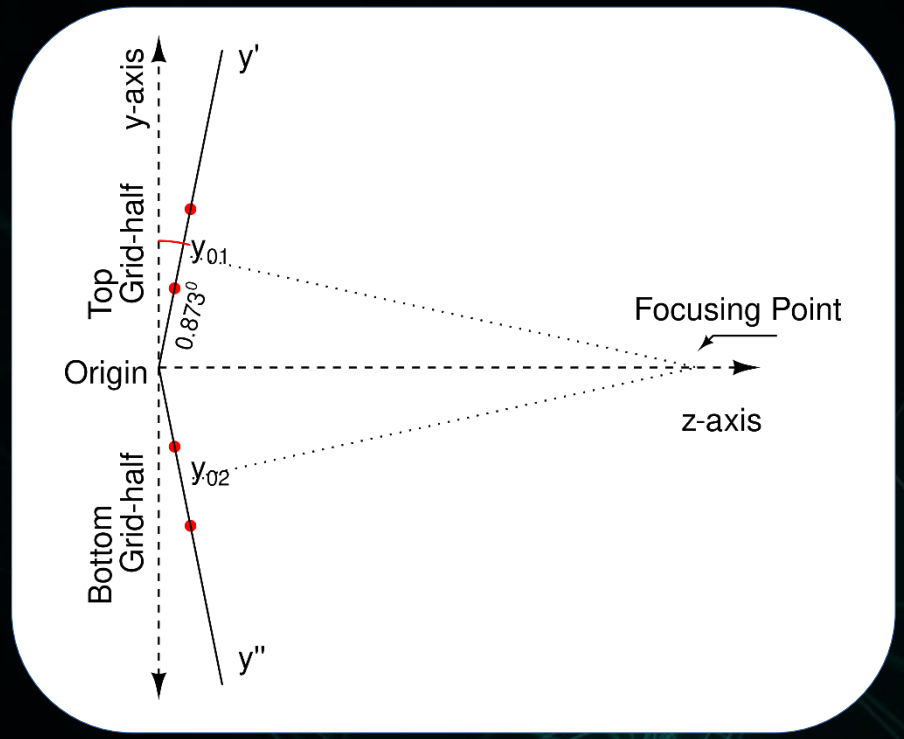

Figure 13: Schematic for grid axes transformation to lab frame for ROBIN geometry

The top grid(y') and the bottom grid(y'') are required to be transformed to lab frames before implementing to the equation for intensity distribution [7].

The transformation for bottom grid will be:

$$y_1 = (y'-y_{01}\cos(\theta))\cos(\theta)+(z'-y_{01}\sin(\theta))\sin(\theta) \quad ...(9a)$$

$$z_1 = -(y'-y_{01}\cos(\theta))\sin(\theta)+(z'-y_{01}\sin(\theta))\cos(\theta) \quad ...(9b)$$

The transformation for top grid will be:

$$y_2 = (y'+y_{02}\cos(\theta))\cos(\theta)-(z'-y_{02}\sin(\theta))\sin(\theta) \quad ...(10a)$$

$$z_2 = (y'+y_{02}\cos(\theta))\sin(\theta)+(z'-y_{02}\sin(\theta))\cos(\theta) \quad ...(10b)$$

The x-axis remains unchanged for both the cases as there is no angular constraints along x-axis.

7. Liang, Lizhen, et al . "Calculation of beam intensity distribution for the neutral beam injection in EAST." Plasma Science and Technology 13, no. 4 (2011): 502.

Beam Modelling

Equation-6 may be solved analytically using the geometry of grounding grid as limits of integral, which reduces to:

$$I_{beam} = (I/[32\, w \times l]) * \{ Erf[(W-x)/a_x] + Erf[(W+x)/a_x] \} * \{ Erf[(L-y)/a_y] + Erf[(L+y)/a_y] \} \quad \ldots(7)$$

- Coordinate transformation for Top Grid
- Coordinate transformation for Bottom Grid
- Lab Frame Coordinates as per ROBIN
- Substituting into equation-7
- Numerical calculation for $(512 \times 512 \times 3072)_{mm}$ spatial volume

Where, the total extraction area of a single grid half is $2W \times 2L = 115.79\ mm \times 71.31\ mm$, and the form of Erf is:

$$Erf(k) = (2/\sqrt{\pi}) \int_0^k \exp(-x^2)\, dx \quad \ldots(8)$$

The numerical resolution for solving was kept at 1 mm per cell and was solved for 3072mm(z) down the beamline with $512 \times 512\ mm^2$ (x-y surface).

Simulation Results

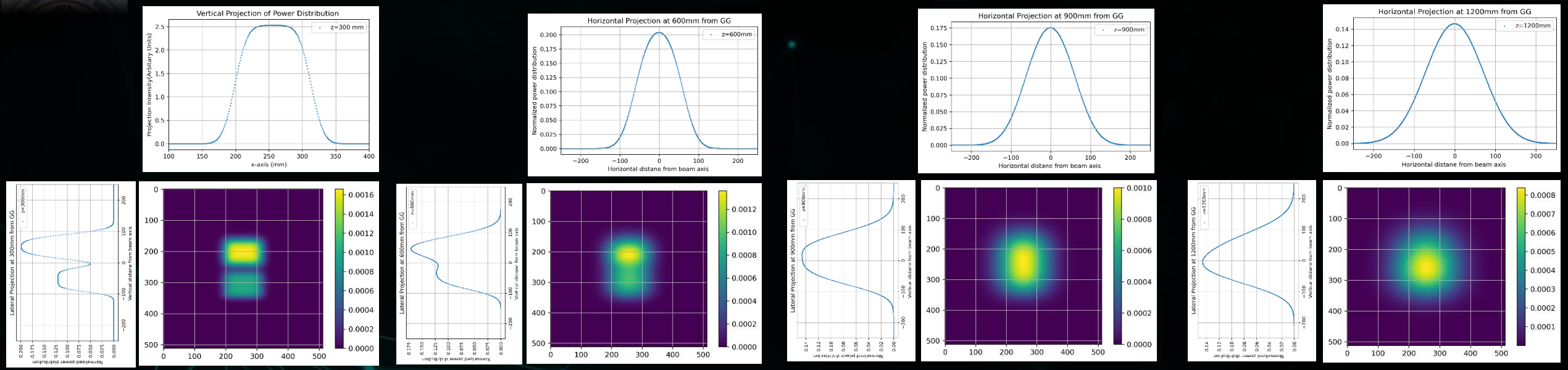

(a) (b) (c) (d)

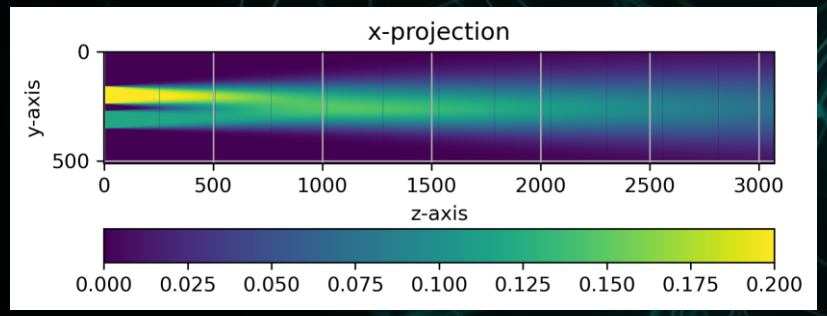

(e)

Simulation Parameters

$\alpha = 4^0$

$\beta_1 = 3.7^0, \beta_2 = 2.7^0$

Asymmetry(I_2/I_1) = 0.6

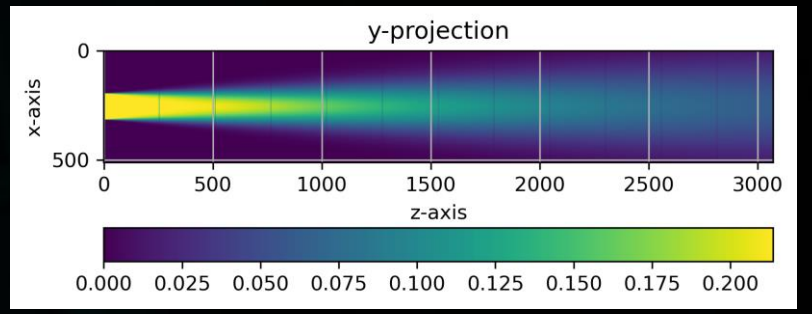

(f)

Figure 14: The projection of power distribution along all three dimensions are presented at a) z=300 mm, b) z=600 mm, c) z=900 mm, d) z=1200 mm from the GG, e) lateral projection f) top projection for the complete beamline.

Co-relating the Results

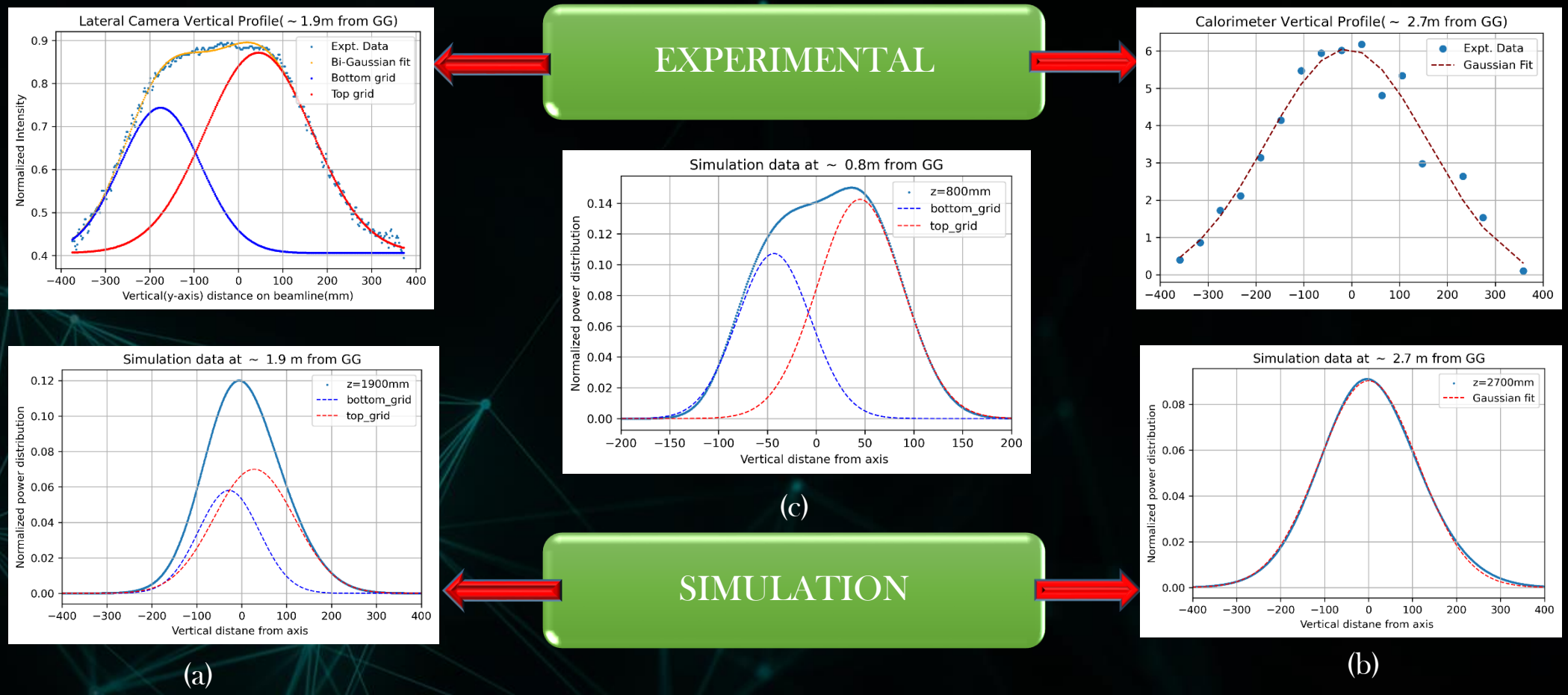

Figure 15: Comparison of simulation and experimental plots for a) the lateral camera at 1.9 m b) the calorimeter at 2.7m from the Grounded Grid or the simulation origin and c) the observed mergence in the simulation .

Summary

A bi-Gaussian distribution with flat top and asymmetric wings indicating two unmerged beams from grid-halves with asymmetric parameters was observed by lateral camera along beamline.

Individual beam-group parameters were resolved. The variation of divergence showed similar trend as observed by the calorimeter for an extraction voltage sweep.

For probing more into the mergence phenomena, a numerical simulation was modelled using an approach suggested by Kim and Whealton, modified according to ROBIN geometry.

The simulation was fed with parameters observed from the lateral camera. The intensity distribution projections were compared with experimentally observed profiles.

References

1. M. Bandyopadhyay, et al , “Overview of diagnostics on a small-scale RF source for fusion (ROBIN) and the one planned for the diagnostic beam for ITER.” Rev Sci Instrum 1 February 2022; 93 (2): 023504. https://doi.org/10.1063/5.0076009 .
2. M. Ugoletti, et al , “Visible cameras as a non-invasive diagnostic to study negative ion beam properties.” Rev Sci Instrum 1 April 2021, 92 (4): 043302, https://doi.org/10.1063/5.0038911 .
3. Pandya, Kaushal, et al, “First results from negative ion beam extraction in ROBIN in surface mode.” In AIP Conference proceedings, vol. 1869, no. 1. AIP Publishing, 2017, https://doi.org/10.1063/1.4995729.
4. D. Borah, et al , “Design of tomographic diagnostic system for Indian Test Facility (INTF) neutral beam injector.” Fusion Engineering and Design, Volume 148, 2019, 111255, ISSN 0920-3796, https://doi.org/10.1016/j.fusengdes.2019.111255.
5. Deka, A. J., et al , “Evaluation of beam divergence of a negative hydrogen ion beam using Doppler shift spectroscopy diagnostics.” Journal of Applied Physics 123, no. 4 (2018), https://doi.org/10.1063/1.5001697.
6. Kim, Jinchoon, and J. H. Whealton. “Beam intensity distributions in neutral beam injection systems.” Nuclear instruments and methods 141, no. 2 (1977): 187-191, https://doi.org/10.1016/0029-554X(77)90767-4.
7. Liang, Lizhen, et al . "Calculation of beam intensity distribution for the neutral beam injection in EAST." Plasma Science and Technology 13, no. 4 (2011): 502, https://doi.org/10.1088/1009-0630/13/4/22 .
8. R. Pasqualotto, et al, “Design of a visible tomography diagnostic for negative ion RF source SPIDER.” Fusion Engineering and Design, Volume 88, Issues6–8, 2013, Pages 1253-1256ISSN 0920-3796, https://doi.org/10.1016/j.fusengdes.2013.02.009.
9. M. Brombin, et al, “The tomographic diagnostic of ITER neutral beam injector.” Nucl. Fusion 53 053009, https://10.1088/0029-5515/53/5/053009 .

The Brief Schematic of ROBIN

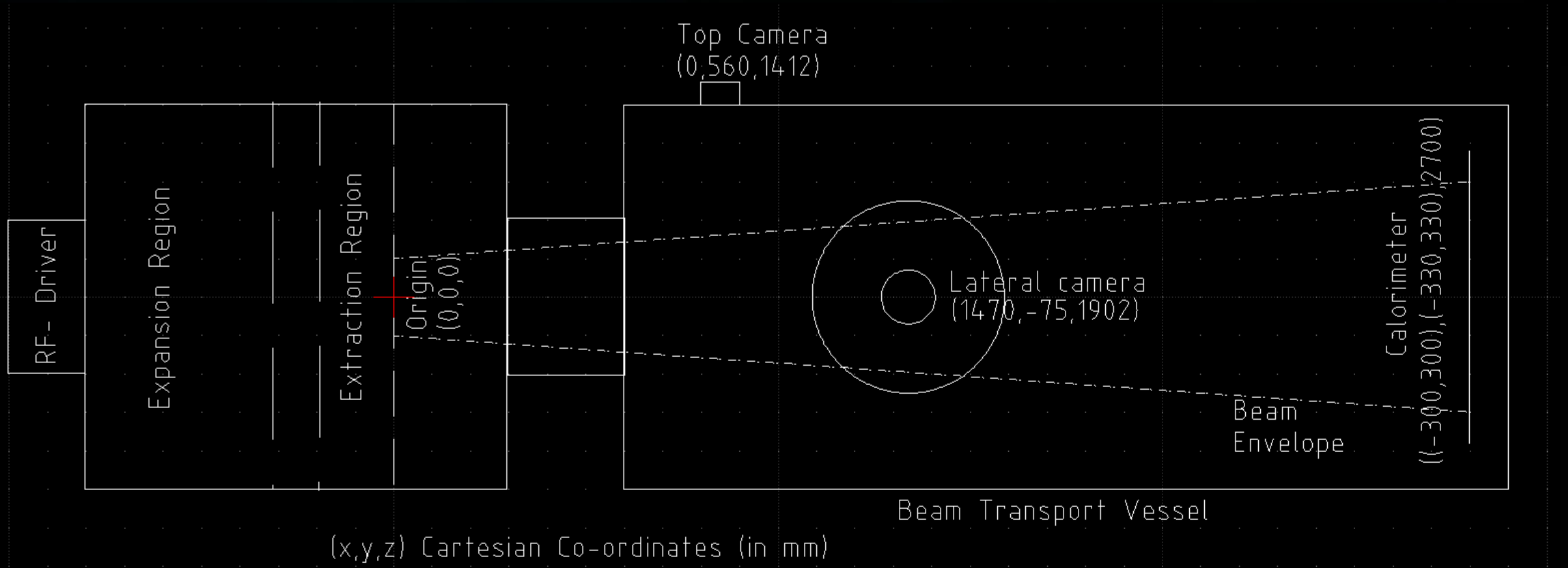

Perspective projection(Pixel Mapping)